TWMS J. App. and Eng. Math. V.15, N.2, 2025, pp. 319-334

HYBRID THE SINE–COSINE WAVELET AND FINITE DIFFERENCE METHOD FOR SOLVING THE NONLINEAR BELOUSOV–ZHABOTINSKY REACTION SYSTEM

S. FOADIAN[1*], R. POURGHOLI[2], §

Abstract. In this paper, a numerical method for solving the nonlinear Belousov–Zhabotinsky reaction system is proposed. The method is based on hybrid function approximations. In the solution process, the time derivative is discretized by the finite difference method, the spatial discretization is made by Sine–Cosine wavelets, and the nonlinear terms are linearized by the quasilinearization technique. Also, the convergence analysis of the proposed method has been discussed. Finally, to show the efficiency and accuracy of the method in solving this system, an illustrative example is included and the results are compared with the Haar wavelet method.

Keywords: Nonlinear Belousov–Zhabotinsky system, Sine–Cosine wavelets method, Finite difference method, Operational matrix, Convergence analysis.

AMS Subject Classification: 65Nxx, 65T60, 74G15

1. Introduction

Nonlinear phenomena have an important place in many areas of science and engineering. Particularly, nonlinear chemical reactions can be widely seen in various fields, such as biological and chemical physics. Especially there has been considerable interest in both biochemical and biological systems resulting in sustained oscillation. For this reason, it has become more important to seek solutions for these kinds of nonlinear phenomena.

One of these nonlinear natural phenomena is the Belousov–Zhabotinsky chemical reaction. Most research work on oscillatory behavior in nonequilibrium dynamics was developed based on the discovery of a particular chemical reaction popularly called the Belousov–Zhabotinsky reaction. The Belousov–Zhabotinsky reaction was first observed in the 1950s by a Russian biochemist named *Boris Belousov* who attempted to simulate the Krebs cycle in vitro. His work came to light through research findings of *A. M. Zhabotinsky* in the 1960's [1, 2, 3]. Nowadays, the Belousov–Zhabotinsky reaction system is generally referred to as the chemical reaction in which an organic substrate is oxidized in the presence

[1,2] School of Mathematics and Computer Science, Damghan University, Damghan, Iran.
e-mail: s.foadian@std.du.ac.ir; https://orcid.org/0000-0001-7091-1254.
e-mail: pourgholi@du.ac.ir; https://orcid.org/0000-0003-4111-5130.
[*] Corresponding author.
§ Manuscript received: August 09, 2023; accepted: December 18, 2023.
TWMS Journal of Applied and Engineering Mathematics, Vol.15, No.2;

of acid by bromate ions with transition metal ions. The Belousov–Zhabotinsky reaction has generated a lot of research attention in the area of applied sciences, most importantly in the field of nonlinear dynamics by theorists interested in modeling complex patterns in biological systems. The Belousov–Zhabotinsky reaction is known to have manifested into various complex dynamic phenomena such as self-replicating patterns, stripes, spots, and mitotic spots, as well as other unusual chaotic structures. The Belousov–Zhabotinsky is likely the most widely studied reaction both theoretically and experimentally [4]. Akinyemi, in [5], investigates numerical solutions to this model with Caputo fractional time derivative. In [6], the operator splitting method has been presented for analysis of the Noyes–Field model for the nonlinear Belousov–Zhabotinsky reaction.

In this paper, we investigate numerical solutions to this nonlinear oscillatory system as

$$\begin{cases} \Phi_t = \Phi_{xx} + \alpha\Psi + \Phi - \Phi^2 - \alpha\Phi\Psi, \\ \Psi_t = \Psi_{xx} + \beta\Psi - \beta\Phi\Psi, \end{cases} \tag{1}$$

with the initial conditions

$$\Phi(x,0) = \rho_1(x), \qquad \Psi(x,0) = \rho_2(x), \qquad 0 \le x \le 1, \tag{2}$$

and the boundary conditions

$$\begin{aligned} &\Phi(0,t) = f_1(t), \quad \Phi(1,t) = f_2(t), \quad 0 \le t \le T^*, \\ &\Psi(0,t) = g_1(t), \quad \Psi(1,t) = g_2(t), \quad 0 \le t \le T^*, \end{aligned} \tag{3}$$

where α and $\beta \neq 1$ are positive parameters, $\rho_1(x)$, $\rho_2(x)$, $f_1(t)$, $f_2(t)$, $g_1(t)$, and $g_2(t)$, are considered as known differentiable functions and T^* denotes a positive constant as the final time. The numerical method is based upon hybrid function approximations with the finite difference and Sine–Cosine wavelets method.

The wavelet methods have become a matter of attention lately in solving differential equations numerically, and they were first applied to solving differential equations in the early 1990s [7, 8]. In the present paper, we use the Sine–Cosine wavelets method. One of the strengths of this method is the orthogonality and compact support of the basis functions used in their construction. In addition, because the number of mother wavelet elements is limited to one, we do not see the growth of computational complexity. Azizi and Pourgholi [9] have used Sine–Cosine wavelets to solve Drinfel'd–Sokolov–Wilson system. Idrees Caputo–Hadamard fractional differential equations In [11], a Sine–Cosine wavelet method has been employed to solve Caputo–Hadamard fractional differential equations. The numerical evaluation of the Hankel transform for seismology using the Sine–Cosine wavelets approach has been given in [12].

The rest of this study is organized into the following sections. In Section 2, a review of the Sine–Cosine wavelets, including: the properties of the Sine–Cosine wavelets, orthonormal basis functions, function approximation, and the convergence analysis of this method are discussed. In Section 3, the application of the Sine–Cosine wavelet method to get numerical solutions of system (1) is presented. The numerical computation and results are made in Section 4. Finally, concluding remarks are drawn in Section 5.

2. A Review of the Sine–Cosine wavelets

In this section, individually, we present the properties of the Sine–Cosine wavelets, orthonormal basis functions, function approximation, and the convergence analysis of this method.

2.1. **The Sine–Cosine wavelets.** Wavelets are useful mathematical functions constructed from the dilation and translation of a single function called the mother wavelet, which can be denoted by $\mathcal{W}(x)$. Assuming that the expansion parameter e and the translation parameter d are considered, we have the continuous wavelets family as follows [13]

$$\mathcal{M}_{e,d}(x) = |e|^{-\frac{1}{2}}\mathcal{W}\Big(\frac{x-d}{e}\Big), \qquad e,d \in \mathbb{R}, \quad e \neq 0.$$

If the parameters e and d are restricted to take values $e = e_0^{-\kappa}$ and $d = \iota d_0 e_0^{-\kappa}$, where $e_0 > 1$, $d_0 > 0$, a family of discrete wavelets is obtained as

$$\mathcal{M}_{\kappa,\iota}(x) = |e_0|^{\frac{\kappa}{2}}\mathcal{W}(e_0^{\kappa}x - \iota d_0), \tag{4}$$

where ι and κ are positive integers. The set $\{\mathcal{M}_{\kappa,\iota}(x)\}$ in (4), forms a wavelet basis for $\mathscr{L}^2(\mathbb{R})$. Especially, if $e_0 = 2$ and $d_0 = 1$, the set $\{\mathcal{M}_{\kappa,\iota}(x)\}$ forms an orthonormal basis.

Sine–Cosine wavelets are defined on interval $0 \leq x \leq 1$ as [12]

$$\mathcal{M}_{\iota,\lambda}(x) = \begin{cases} 2^{\frac{\kappa+1}{2}}\mathscr{H}_{\lambda}(2^{\kappa}x - \iota), & x \in [\frac{\iota}{2^{\kappa}}, \frac{\iota+1}{2^{\kappa}}), \\ 0, & \text{elsewhere.} \end{cases} \tag{5}$$

where $\kappa = \{0\} \cup \mathbb{N}$, $\iota = 0, 1, 2, \ldots, 2^{\kappa} - 1$, also,

$$\mathscr{H}_{\lambda}(x) = \begin{cases} \frac{1}{\sqrt{2}}, & \text{if } \lambda = 0, \\ \cos(2\lambda\pi x), & \text{if } \lambda = 1, 2, \ldots, \ell^*, \\ \sin(2(\lambda - \ell^*)\pi x), & \text{if } \lambda = \ell^* + 1, \ell^* + 2, \ldots, 2\ell^*, \end{cases} \tag{6}$$

where ℓ^* is any positive integer.

2.2. **Orthonormal basis functions.** In this subsection, the orthonormal basis functions for Sine–Cosine wavelets by fixing $\kappa = 1$ and $\ell^* = 2$ are obtained in the following for $0 \leq x < \frac{1}{2}$:

$$\begin{cases} \mathcal{M}_{0,0}(x) = \sqrt{2}, \\ \mathcal{M}_{0,1}(x) = 2\cos(4\pi x), \\ \mathcal{M}_{0,2}(x) = 2\cos(8\pi x), \\ \mathcal{M}_{0,3}(x) = 2\sin(4\pi x), \\ \mathcal{M}_{0,4}(x) = 2\sin(8\pi x), \end{cases}$$

and for $\frac{1}{2} \leq x < 1$:

$$\begin{cases} \mathcal{M}_{1,0}(x) = \sqrt{2}, \\ \mathcal{M}_{1,1}(x) = 2\cos(4\pi x - 2\pi), \\ \mathcal{M}_{1,2}(x) = 2\cos(8\pi x - 4\pi), \\ \mathcal{M}_{1,3}(x) = 2\sin(4\pi x - 2\pi), \\ \mathcal{M}_{1,4}(x) = 2\sin(8\pi x - 4\pi). \end{cases}$$

For instance, the graphs of $\mathcal{M}_{\iota,\lambda}(x)$ for $\kappa = \ell^* = 1$, with the collocation points

$$x_i = \frac{2i-1}{2\mathtt{M}}, \qquad i = 1, 2, \ldots, \mathtt{M} = 2^{\kappa}(2\ell^* + 1), \tag{7}$$

are shown in Figure 1.

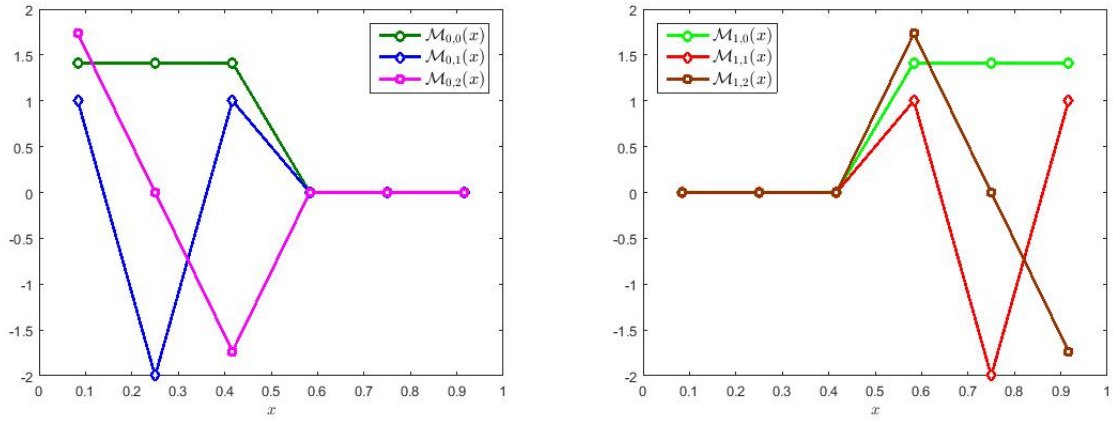

FIGURE 1. The graphs of $\mathcal{M}_{\iota,\lambda}(x)$ for $\kappa = 1$ and $\ell^* = 1$.

2.3. **Function approximation.** Our aim in this subsection is to apply the Sine–Cosine wavelets for solving system (1). Since Sine–Cosine wavelets have compact support and are an orthonormal basis for $\mathscr{L}^2([0,1))$, Hence, it should be noted that any function $\mathcal{U}(x) \in \mathscr{L}^2([0,1))$ can be expanded into the Sine–Cosine wavelets as infinite series as follows

$$\mathcal{U}(x) = \sum_{\iota=0}^{\infty} \sum_{\lambda=0}^{2\ell^*} c_{\iota,\lambda} \mathcal{M}_{\iota,\lambda}(x), \tag{8}$$

where the wavelet coefficients $c_{\iota,\lambda}$ are defined by $c_{\iota,\lambda} =< \mathcal{U}, \mathcal{M}_{\iota,\lambda} >$, where $< \cdot, \cdot >$ denotes the inner product.
In practical purpose, for approximating unknown function $\mathcal{U}(x) \in \mathscr{L}^2([0,1))$, the finite terms of the Sine–Cosine wavelets series are needed; hence, by truncating the infinite series (8) at level $\iota = 2^\kappa - 1$, we obtain an approximate representation for $\mathcal{U}(x)$ as follows

$$\mathcal{U}(x) \simeq \sum_{\iota=0}^{2^\kappa-1} \sum_{\lambda=0}^{2\ell^*} c_{\iota,\lambda} \mathcal{M}_{\iota,\lambda}(x) = \mathbf{C}^T \mathbf{\Pi}(x), \tag{9}$$

where $\mathbf{C}$ and $\mathbf{\Pi}$ are $(\mathtt{M} \times 1)$-vectors and are given by

$$\mathbf{C} = \Big[c_{0,0}, c_{0,1}, \ldots, c_{0,2\ell^*}, c_{1,0}, c_{1,1}, \ldots, c_{1,2\ell^*}, \ldots\ldots, c_{2^\kappa-1,0}, c_{2^\kappa-1,1}, \ldots, c_{2^\kappa-1,2\ell^*}\Big]^T, \tag{10}$$

$$\mathbf{\Pi} = \Big[\mathcal{M}_{0,0}(x), \ldots, \mathcal{M}_{0,2\ell^*}(x), \mathcal{M}_{1,0}(x), \ldots, \mathcal{M}_{1,2\ell^*}(x), \ldots\ldots, \mathcal{M}_{2^\kappa-1,0}(x), \ldots, \mathcal{M}_{2^\kappa-1,2\ell^*}(x)\Big]^T. \tag{11}$$

Considering the collocation points (7), the Sine–Cosine wavelets matrix $\mathbf{\Pi}_{\mathtt{M}\times\mathtt{M}}$ is given by

$$\mathbf{\Pi}_{\mathtt{M}\times\mathtt{M}} = \left[\mathbf{\Pi}\Big(\frac{1}{2\mathtt{M}}\Big), \mathbf{\Pi}\Big(\frac{3}{2\mathtt{M}}\Big), \ldots, \mathbf{\Pi}\Big(\frac{2\mathtt{M}-1}{2\mathtt{M}}\Big)\right],$$

in other words

$$\mathbf{\Pi}_{\mathtt{M}\times\mathtt{M}}=\begin{bmatrix}
\mathcal{M}_{0,0}(\frac{1}{2\mathtt{M}}) & \mathcal{M}_{0,0}(\frac{3}{2\mathtt{M}}) & \dots & \mathcal{M}_{0,0}(\frac{2\mathtt{M}-1}{2\mathtt{M}})\\
\mathcal{M}_{0,1}(\frac{1}{2\mathtt{M}}) & \mathcal{M}_{0,1}(\frac{3}{2\mathtt{M}}) & \dots & \mathcal{M}_{0,1}(\frac{2\mathtt{M}-1}{2\mathtt{M}})\\
\vdots & \vdots & \dots & \vdots\\
\mathcal{M}_{0,2\ell^*}(\frac{1}{2\mathtt{M}}) & \mathcal{M}_{0,2\ell^*}(\frac{3}{2\mathtt{M}}) & \dots & \mathcal{M}_{0,2\ell^*}(\frac{2\mathtt{M}-1}{2\mathtt{M}})\\
\mathcal{M}_{1,0}(\frac{1}{2\mathtt{M}}) & \mathcal{M}_{1,0}(\frac{3}{2\mathtt{M}}) & \dots & \mathcal{M}_{1,0}(\frac{2\mathtt{M}-1}{2\mathtt{M}})\\
\mathcal{M}_{1,1}(\frac{1}{2\mathtt{M}}) & \mathcal{M}_{1,1}(\frac{3}{2\mathtt{M}}) & \dots & \mathcal{M}_{1,1}(\frac{2\mathtt{M}-1}{2\mathtt{M}})\\
\vdots & \vdots & \dots & \vdots\\
\mathcal{M}_{1,2\ell^*}(\frac{1}{2\mathtt{M}}) & \mathcal{M}_{1,2\ell^*}(\frac{3}{2\mathtt{M}}) & \dots & \mathcal{M}_{1,2\ell^*}(\frac{2\mathtt{M}-1}{2\mathtt{M}})\\
\vdots & \vdots & \dots & \vdots\\
\vdots & \vdots & \dots & \vdots\\
\mathcal{M}_{2^\kappa-1,0}(\frac{1}{2\mathtt{M}}) & \mathcal{M}_{2^\kappa-1,0}(\frac{3}{2\mathtt{M}}) & \dots & \mathcal{M}_{2^\kappa-1,0}(\frac{2\mathtt{M}-1}{2\mathtt{M}})\\
\mathcal{M}_{2^\kappa-1,1}(\frac{1}{2\mathtt{M}}) & \mathcal{M}_{2^\kappa-1,1}(\frac{3}{2\mathtt{M}}) & \dots & \mathcal{M}_{2^\kappa-1,1}(\frac{2\mathtt{M}-1}{2\mathtt{M}})\\
\vdots & \vdots & \dots & \vdots\\
\mathcal{M}_{2^\kappa-1,2\ell^*}(\frac{1}{2\mathtt{M}}) & \mathcal{M}_{2^\kappa-1,2\ell^*}(\frac{3}{2\mathtt{M}}) & \dots & \mathcal{M}_{2^\kappa-1,2\ell^*}(\frac{2\mathtt{M}-1}{2\mathtt{M}})
\end{bmatrix}. \tag{12}$$

For example, when $\kappa=1$ and $\ell^*=2$, $\mathbf{\Pi}_{10\times10}$ is given as follows

$$\mathbf{\Pi}_{10\times10}=\begin{bmatrix}
1.4142 & 1.4142 & 1.4142 & 1.4142 & 1.4142 & 0 & 0 & 0 & 0 & 0\\
1.6180 & -0.6180 & -2.0000 & -0.6180 & 1.6180 & 0 & 0 & 0 & 0 & 0\\
0.6180 & -1.6180 & 2.0000 & -1.6180 & 0.6180 & 0 & 0 & 0 & 0 & 0\\
1.1756 & 1.9021 & 0.0000 & -1.9021 & -1.1756 & 0 & 0 & 0 & 0 & 0\\
1.9021 & -1.1756 & -0.0000 & 1.1756 & -1.9021 & 0 & 0 & 0 & 0 & 0\\
0 & 0 & 0 & 0 & 0 & 1.4142 & 1.4142 & 1.4142 & 1.4142 & 1.4142\\
0 & 0 & 0 & 0 & 0 & 1.6180 & -0.6180 & -2.0000 & -0.6180 & 1.6180\\
0 & 0 & 0 & 0 & 0 & 0.6180 & -1.6180 & 2.0000 & -1.6180 & 0.6180\\
0 & 0 & 0 & 0 & 0 & 1.1756 & 1.9021 & 0.0000 & -1.9021 & -1.1756\\
0 & 0 & 0 & 0 & 0 & 1.9021 & -1.1756 & -0.0000 & 1.1756 & -1.9021
\end{bmatrix}.$$

The integration of the vector $\mathbf{\Pi}(x)$ where defined in equation (11), can be calculated as follows

$$\int_0^x \mathbf{\Pi}(\tau)\,d\tau=\mathcal{Q}\mathbf{\Pi}(x),$$

where the $\mathtt{M}\times\mathtt{M}$ operational matrix $\mathcal{Q}$ is given by

$$\mathcal{Q}=\frac{1}{2^{\frac{\kappa+1}{2}}}\begin{pmatrix}
\mathcal{X} & \mathcal{Y} & \cdots & \mathcal{Y}\\
0 & \mathcal{X} & \cdots & \mathcal{Y}\\
\vdots & \vdots & \ddots & \vdots\\
0 & 0 & \cdots & \mathcal{X}
\end{pmatrix}.$$

The $(2\ell^*+1)\times(2\ell^*+1)$-matrices $\mathcal{X}$ and $\mathcal{Y}$ are defined as follows

$$\mathcal{X}=\begin{pmatrix} \frac{1}{2} & 0 & 0 & \cdots & 0 & -\frac{1}{\pi} & -\frac{1}{2\pi} & \cdots & -\frac{1}{\ell^*\pi} \\ 0 & 0 & 0 & \cdots & 0 & \frac{1}{2\pi} & 0 & \cdots & 0 \\ 0 & 0 & 0 & \cdots & 0 & 0 & \frac{1}{4\pi} & \cdots & 0 \\ \vdots & \vdots & \vdots & \ddots & \vdots & \vdots & \vdots & \ddots & \vdots \\ 0 & 0 & 0 & \cdots & 0 & 0 & 0 & \cdots & \frac{1}{2\ell^*\pi} \\ \frac{1}{2\pi} & -\frac{1}{2\pi} & 0 & \cdots & 0 & 0 & 0 & \cdots & 0 \\ \frac{1}{4\pi} & 0 & -\frac{1}{4\pi} & \cdots & 0 & 0 & 0 & \cdots & 0 \\ \vdots & \vdots & \vdots & \ddots & \vdots & \vdots & \vdots & \ddots & \vdots \\ \frac{1}{2\ell^*\pi} & 0 & 0 & \cdots & -\frac{1}{2\ell^*\pi} & 0 & 0 & \cdots & 0 \end{pmatrix},$$

$$\mathcal{Y}=\begin{pmatrix} 1 & 0 & 0 & \cdots & 0 \\ 0 & 0 & 0 & \cdots & 0 \\ 0 & 0 & 0 & \cdots & 0 \\ \vdots & \vdots & \vdots & \ddots & \vdots \\ 0 & 0 & 0 & \cdots & 0 \end{pmatrix}.$$

2.4. **Convergence analysis of the Sine–Cosine wavelets.**

Theorem 2.1. *The approximate solution* (9) *converges to* $\mathcal{U}(x)$ *in* (8)*, when* $\kappa\to\infty$.

Proof. Suppose that $\mathcal{J}_{\kappa,\ell^*}$ be a sequence of partial sums of $c_{\iota,\lambda}\mathcal{M}_{\iota,\lambda}(x)$ as

$$\mathcal{J}_{\kappa,\ell^*}(x)=\sum_{\iota=0}^{2^\kappa-1}\sum_{\lambda=0}^{2\ell^*}c_{\iota,\lambda}\mathcal{M}_{\iota,\lambda}(x).$$

We demonstrate $\mathcal{J}_{\kappa,\ell^*}$ is a Cauchy sequence in Hilbert space $\mathscr{L}^2([0,1))$ and then, we show that when $\kappa\to\infty$, $\mathcal{J}_{\kappa,\ell^*}$ converges to $\mathcal{U}(x)$. To do this, first we let $\mathcal{J}_{\kappa',\ell^*}$ be arbitrary sums of $c_{\iota,\lambda}\mathcal{M}_{\iota,\lambda}(x)$ with $\kappa>\kappa'$. Therefore,

$$\begin{aligned}\left\|\mathcal{J}_{\kappa,\ell^*}-\mathcal{J}_{\kappa',\ell^*}\right\|^2&=\left\|\sum_{\iota=2^{\kappa'}}^{2^\kappa-1}\sum_{\lambda=0}^{2\ell^*}c_{\iota,\lambda}\mathcal{M}_{\iota,\lambda}(x)\right\|^2\\&=\left\langle\sum_{\iota=2^{\kappa'}}^{2^\kappa-1}\sum_{\lambda=0}^{2\ell^*}c_{\iota,\lambda}\mathcal{M}_{\iota,\lambda}(x),\sum_{\iota'=2^{\kappa'}}^{2^\kappa-1}\sum_{\lambda'=0}^{2\ell^*}c_{\iota',\lambda'}\mathcal{M}_{\iota',\lambda'}(x)\right\rangle\\&=\sum_{\iota=2^{\kappa'}}^{2^\kappa-1}\sum_{\lambda=0}^{2\ell^*}\sum_{\iota'=2^{\kappa'}}^{2^\kappa-1}\sum_{\lambda'=0}^{2\ell^*}c_{\iota,\lambda}\bar{c}_{\iota',\lambda'}\left\langle\mathcal{M}_{\iota,\lambda}(x),\mathcal{M}_{\iota',\lambda'}(x)\right\rangle\\&=\sum_{\iota=2^{\kappa'}}^{2^\kappa-1}\sum_{\lambda=0}^{2\ell^*}|c_{\iota,\lambda}|^2.\end{aligned}$$

We have $\sum_{\iota=0}^{\infty}\sum_{\lambda=0}^{2\ell^*}|c_{\iota,\lambda}|^2$, is convergent (From Bessel's inequality). So, when $\kappa\to\infty$, we have

$$\left\|\mathcal{J}_{\kappa,\ell^*}-\mathcal{J}_{\kappa',\ell^*}\right\|^2\to 0.$$

This result demonstrates that $\mathcal{J}_{\kappa,\ell^*}$ is a Cauchy sequence, and so, it converges to a function $\mathcal{Z}(x) \in \mathscr{L}^2([0,1))$. Now, it is enough to show $\mathcal{Z}(x) = \mathcal{U}(x)$.

$$\begin{aligned}\Big\langle \mathcal{Z} - \mathcal{U}, \mathcal{M}_{\iota,\lambda} \Big\rangle &= \Big\langle \mathcal{Z}, \mathcal{M}_{\iota,\lambda} \Big\rangle - \Big\langle \mathcal{U}, \mathcal{M}_{\iota,\lambda} \Big\rangle \\ &= \lim_{\kappa\to\infty} \Big\langle \mathcal{J}_{\kappa,\ell^*}, \mathcal{M}_{\iota,\lambda} \Big\rangle - c_{\iota,\lambda} \\ &= c_{\iota,\lambda} - c_{\iota,\lambda} = 0.\end{aligned}$$

Hence, $\sum_{\iota=0}^{2^\kappa-1} \sum_{\lambda=0}^{2\ell^*} c_{\iota,\lambda}\mathcal{M}_{\iota,\lambda}(x)$ converges to $\mathcal{U}(x)$ when $\kappa \to \infty$ and this completes the proof. □

3. Description of the proposed method

In this section, we present the application of the Sine–Cosine wavelet method to get numerical solutions of system (1), with initial and boundary conditions (2) and (3), respectively.

Firstly, for discretizing equations of system (1), we substitute Φ_t and Ψ_t by forward finite difference and also use time average for Φ_{xx}, Ψ_{xx}, Ψ, Φ, Φ^2, $\Phi\Psi$ terms, so we get the following relations

$$\begin{cases} \dfrac{\Phi(x,t_{j+1}) - \Phi(x,t_j)}{\hbar_t} = \dfrac{\Phi_{xx}(x,t_{j+1}) + \Phi_{xx}(x,t_j)}{2} + \alpha\dfrac{\Psi(x,t_{j+1}) + \Psi(x,t_j)}{2} \\ \qquad + \dfrac{\Phi(x,t_{j+1}) + \Phi(x,t_j)}{2} - \dfrac{\Phi^2(x,t_{j+1}) + \Phi^2(x,t_j)}{2} \\ \qquad - \alpha\dfrac{\Phi\Psi(x,t_{j+1}) + \Phi\Psi(x,t_j)}{2}, \\ \dfrac{\Psi(x,t_{j+1}) - \Psi(x,t_j)}{\hbar_t} = \dfrac{\Psi_{xx}(x,t_{j+1}) + \Psi_{xx}(x,t_j)}{2} + \beta\dfrac{\Psi(x,t_{j+1}) + \Psi(x,t_j)}{2} \\ \qquad - \beta\dfrac{\Phi\Psi(x,t_{j+1}) + \Phi\Psi(x,t_j)}{2}, \end{cases} \tag{13}$$

where $\hbar_t$ is the time step. If we use the linearizations

$$2\Phi(x,t_j)\Phi(x,t_{j+1}) - \Phi^2(x,t_j),$$

and

$$\Psi(x,t_j)\Phi(x,t_{j+1}) + \Phi(x,t_j)\Psi(x,t_{j+1}) - \Phi(x,t_j)\Psi(x,t_j),$$

which is similar to the quasilinearization technique [14], instead of nonlinear terms $\Phi^2(x,t_{j+1})$ and $\Phi\Psi(x,t_{j+1})$, respectively, and simplify the equations of system (13), we obtain

$$\begin{cases} \Gamma_1\Phi(x,t_{j+1}) + \Gamma_2\Psi(x,t_{j+1}) - \theta\Phi_{xx}(x,t_{j+1}) = \mathcal{B}_1, \\ \Gamma_3\Phi(x,t_{j+1}) + \Gamma_4\Psi(x,t_{j+1}) - \theta\Psi_{xx}(x,t_{j+1}) = \mathcal{B}_2, \end{cases} \tag{14}$$

where $\theta = \frac{\hbar_t}{2}$ and

$$\begin{aligned} \Gamma_1 &= 1 + \theta - 2\theta\Phi(x,t_j) - \alpha\theta\Psi(x,t_j), \\ \Gamma_2 &= \alpha\theta\Big(1 - \Phi(x,t_j)\Big), \\ \Gamma_3 &= \beta\theta\Psi(x,t_j), \\ \Gamma_4 &= 1 - \beta\theta\Big(1 - \Phi(x,t_j)\Big), \\ \mathcal{B}_1 &= \theta\Phi_{xx}(x,t_j) + (1+\theta)\Phi(x,t_j) + \alpha\theta\Psi(x,t_j), \\ \mathcal{B}_2 &= \theta\Psi_{xx}(x,t_j) + (1+\beta\theta)\Psi(x,t_j). \end{aligned}$$

3.1. Sine–Cosine wavelet method for spatial–discretization.

In this subsection, we introduce the discretization of spatial derivatives that appeared in system (14). For this, we divide the interval $[0, T^*]$ into $\mathtt{N}$ subinterval with the length $\hbar_t = \frac{T^*}{\mathtt{N}}$ and denote $t_j = (j-1)\hbar_t$, $j = 1, 2, \ldots, \mathtt{N}+1$. We assume that $\Phi_{xx}(x,t_{j+1})$ and $\Psi_{xx}(x,t_{j+1})$ can be expanded in terms of Sine–Cosine wavelets as

$$\Phi_{xx}(x,t_{j+1}) \simeq \sum_{\iota=0}^{2^\kappa-1} \sum_{\lambda=0}^{2\ell^*} c_{\iota,\lambda}\mathcal{M}_{\iota,\lambda}(x) = \mathbf{C}^T\mathbf{\Pi}(x), \tag{15}$$

$$\Psi_{xx}(x,t_{j+1}) \simeq \sum_{\iota=0}^{2^\kappa-1} \sum_{\lambda=0}^{2\ell^*} d_{\iota,\lambda}\mathcal{M}_{\iota,\lambda}(x) = \mathbf{D}^T\mathbf{\Pi}(x). \tag{16}$$

By integrating equations (15) and (16), twice times with respect to x from 0 to x, we get the following equations

$$\Phi(x,t_{j+1}) = \mathbf{C}^T\mathcal{Q}^2\mathbf{\Pi}(x) + \Phi(0,t_{j+1}) + x\Phi_x(0,t_{j+1}), \tag{17}$$
$$\Psi(x,t_{j+1}) = \mathbf{D}^T\mathcal{Q}^2\mathbf{\Pi}(x) + \Psi(0,t_{j+1}) + x\Psi_x(0,t_{j+1}). \tag{18}$$

In equations (17) and (18), the terms $\Phi_x(0,t_{j+1})$ and $\Psi_x(0,t_{j+1})$ are unknown. So, by using the boundary conditions $\Phi(1,t) = f_2(t)$ and $\Psi(1,t) = g_2(t)$ these equations are changed as follows

$$\Phi(x,t_{j+1}) = \mathbf{C}^T\mathcal{Q}^2\mathbf{\Pi}(x) + (1-x)f_1(t_{j+1}) + xf_2(t_{j+1}), \tag{19}$$
$$\Psi(x,t_{j+1}) = \mathbf{D}^T\mathcal{Q}^2\mathbf{\Pi}(x) + (1-x)g_1(t_{j+1}) + xg_2(t_{j+1}). \tag{20}$$

Substituting (19) and (20) into the eqution of system (14), we get

$$\begin{cases} \Big[\Gamma_1\mathcal{Q}^2\mathbf{\Pi}(x) - \theta\mathbf{\Pi}(x)\Big]\mathbf{C}^T + \Big[\Gamma_2\mathcal{Q}^2\mathbf{\Pi}(x)\Big]\mathbf{D}^T = \mathcal{B}_1 - \Gamma_1\Big[(1-x)f_1(t_{j+1}) + xf_2(t_{j+1})\Big] \\ \qquad\qquad - \Gamma_2\Big[(1-x)g_1(t_{j+1}) + xg_2(t_{j+1})\Big], \\ \Big[\Gamma_3\mathcal{Q}^2\mathbf{\Pi}(x)\Big]\mathbf{C}^T + \Big[\Gamma_4\mathcal{Q}^2\mathbf{\Pi}(x) - \theta\mathbf{\Pi}(x)\Big]\mathbf{D}^T = \mathcal{B}_2 - \Gamma_3\Big[(1-x)f_1(t_{j+1}) + xf_2(t_{j+1})\Big] \\ \qquad\qquad - \Gamma_4\Big[(1-x)g_1(t_{j+1}) + xg_2(t_{j+1})\Big]. \end{cases} \tag{21}$$

By evaluating equations of system (21) at the collocation points (7), a linear system of equations for unknown wavelet coefficients $\mathbf{C}$ and $\mathbf{D}$ is derived as follows

$$\begin{cases} \Lambda_1\mathbf{C}^T + \Lambda_2\mathbf{D}^T = \mathcal{G}_1(x_i,t_j), \\ \Lambda_3\mathbf{C}^T + \Lambda_4\mathbf{D}^T = \mathcal{G}_2(x_i,t_j), \end{cases} \tag{22}$$

where

$$\begin{aligned} &\Lambda_1 = \Gamma_1\mathcal{Q}^2\mathbf{\Pi}(x_i) - \theta\mathbf{\Pi}(x_i), \\ &\Lambda_2 = \Gamma_2\mathcal{Q}^2\mathbf{\Pi}(x_i), \\ &\Lambda_3 = \Gamma_3\mathcal{Q}^2\mathbf{\Pi}(x_i), \\ &\Lambda_4 = \Gamma_4\mathcal{Q}^2\mathbf{\Pi}(x_i) - \theta\mathbf{\Pi}(x_i), \\ &\mathcal{G}_1(x_i,t_j) = \mathcal{B}_1 - \Gamma_1\Big[(1-x_i)f_1(t_{j+1}) + x_if_2(t_{j+1})\Big] - \Gamma_2\Big[(1-x_i)g_1(t_{j+1}) + x_ig_2(t_{j+1})\Big], \\ &\mathcal{G}_2(x_i,t_j) = \mathcal{B}_2 - \Gamma_3\Big[(1-x_i)f_1(t_{j+1}) + x_if_2(t_{j+1})\Big] - \Gamma_4\Big[(1-x_i)g_1(t_{j+1}) + x_ig_2(t_{j+1})\Big]. \end{aligned}$$

The linear system (22) can be represented in the matrix form as follows

$$\left[\begin{array}{c:c} \Lambda_1 & \Lambda_2 \\ \hdashline \Lambda_3 & \Lambda_4 \end{array}\right]_{2\mathtt{M}\times 2\mathtt{M}} \left[\begin{array}{c} \mathbf{C} \\ \hdashline \mathbf{D} \end{array}\right]_{2\mathtt{M}\times 1} = \left[\begin{array}{c} \mathcal{G}_1 \\ \hdashline \mathcal{G}_2 \end{array}\right]_{2\mathtt{M}\times 1} \tag{23}$$

This system is solved by using appropriate software and the wavelet coefficients $\mathbf{C}$ and $\mathbf{D}$ are found.
In the following, we provide an Algorithm 1 of the Sine–Cosine wavelets method to obtain a numerical solution of the nonlinear Belousov–Zhabotinsky reaction system.

Algorithm 1 Algorithm for the proposed Sine–Cosine wavelets method

- **Input:** The positive integers κ and ℓ^*.
- Define the Sine–Cosine wavelets $\mathcal{M}_{\iota,\lambda}(x)$ by equation (5).
- Construct the vector $\mathbf{\Pi}_{\mathtt{M}\times 1}$ from (11).
- Construct the Sine–Cosine wavelets matrix $\mathbf{\Pi}_{\mathtt{M}\times\mathtt{M}}$ using the collocation points (7) (matrix (12)).
- Compute the operational matrix $\mathcal{Q}_{\mathtt{M}\times\mathtt{M}}$.
- Define unknown coefficient vectors

$$\mathbf{C}_{\mathtt{M}\times 1} = \Big[c_{0,0}, c_{0,1}, \ldots, c_{0,2\ell^*}, c_{1,0}, c_{1,1}, \ldots, c_{1,2\ell^*}, \ldots\ldots, c_{2^\kappa-1,0}, c_{2^\kappa-1,1}, \ldots, c_{2^\kappa-1,2\ell^*}\Big]^T,$$

  and

$$\mathbf{D}_{\mathtt{M}\times 1} = \Big[d_{0,0}, d_{0,1}, \ldots, d_{0,2\ell^*}, d_{1,0}, d_{1,1}, \ldots, d_{1,2\ell^*}, \ldots\ldots, d_{2^\kappa-1,0}, d_{2^\kappa-1,1}, \ldots, d_{2^\kappa-1,2\ell^*}\Big]^T.$$

- Convert the equations of system (1) into a system of discrete equations by using forward finite difference and also use time average method.
- Convert the obtained equations into a linearized differential equation by using the quasilinearization technique.
- Approximate the highest spatial derivatives function in system (14) by Sine–Cosine wavelets.
- Establish the system of algebraic equations (22).
- Solve the system of algebraic equations in the previous step by any classical method in the appropriate software.
- Substitute the obtained wavelet coefficients $\mathbf{C}$ and $\mathbf{D}$ into (19) and (20).
- **Output:** The approximate solutions $\Phi(x,t)$ and $\Psi(x,t)$ on $[0,1]\times[0,T^*]$.

4. Numerical computation and results

In this section, numerical computation of the nonlinear Belousov–Zhabotinsky reaction equation (1) is obtained. These results and graphical outputs were generated by MATLAB R2015b, and all codes were run on a personal computer.

To show the performance of the proposed method as compared with the exact solution, we used the error norms L_∞, for $0 < x < 1$ and $0 < t \le T^*$ as follows

$$(L_\infty)_\Phi = ||\Phi_{exact}(x,t) - \Phi_{approx}(x,t)||_\infty = \max|\Phi_{exact}(x,t) - \Phi_{approx}(x,t)|,$$
$$(L_\infty)_\Psi = ||\Psi_{exact}(x,t) - \Psi_{approx}(x,t)||_\infty = \max|\Psi_{exact}(x,t) - \Psi_{approx}(x,t)|,$$

and the error norms L_2 as follows

$$(L_2)_\Phi = \sqrt{\hbar_x \sum_{i=1}^{\mathtt{M}} \Big(\Phi_{exact}(x_i,t) - \Phi_{approx}(x_i,t)\Big)^2},$$
$$(L_2)_\Psi = \sqrt{\hbar_x \sum_{i=1}^{\mathtt{M}} \Big(\Psi_{exact}(x_i,t) - \Psi_{approx}(x_i,t)\Big)^2},$$

where $\hbar_x = \frac{1}{\mathtt{M}}$. Also,

$$(L_2)_\Phi = \sqrt{\hbar_t \sum_{j=2}^{\mathtt{N}+1} \Big(\Phi_{exact}(x,t_j) - \Phi_{approx}(x,t_j)\Big)^2},$$
$$(L_2)_\Psi = \sqrt{\hbar_t \sum_{j=2}^{\mathtt{N}+1} \Big(\Psi_{exact}(x,t_j) - \Psi_{approx}(x,t_j)\Big)^2},$$

where $\hbar_t = \frac{T^*}{\mathtt{N}}$.

4.1. **Model problem.** For the implementation of numerical works carried out in section 3, we will consider the nonlinear Belousov–Zhabotinsky reaction equation (1) with the following initial conditions

$$\rho_1(x) = \frac{1}{4}\left[\tanh\Big(\sqrt{\frac{\beta}{24}}x\Big) - 1\right]^2, \qquad \rho_2(x) = \frac{\beta-1}{4\alpha}\left[\tanh\Big(\sqrt{\frac{\beta}{24}}x\Big) - 1\right]^2, \qquad 0 \le x \le 1,$$

and the boundary conditions

$$f_1(t) = \frac{1}{4}\left[\tanh\Big(\frac{5\beta}{12}t\Big) + 1\right]^2, \qquad f_2(t) = \frac{1}{4}\left[\tanh\Big(\sqrt{\frac{\beta}{24}} - \frac{5\beta}{12}t\Big) - 1\right]^2, \qquad 0 \le t \le T^*,$$

$$g_1(t) = \frac{\beta-1}{4\alpha}\left[\tanh\Big(\frac{5\beta}{12}t\Big) + 1\right]^2, \qquad g_2(t) = \frac{\beta-1}{4\alpha}\left[\tanh\Big(\sqrt{\frac{\beta}{24}} - \frac{5\beta}{12}t\Big) - 1\right]^2, \qquad 0 \le t \le T^*.$$

The exact solutions are given in [5] as

$$\Phi(x,t) = \frac{1}{4}\left[\tanh\Big(\sqrt{\frac{\beta}{24}}x - \frac{5\beta}{12}t\Big) - 1\right]^2, \qquad \Psi(x,t) = \frac{\beta-1}{4\alpha}\left[\tanh\Big(\sqrt{\frac{\beta}{24}}x - \frac{5\beta}{12}t\Big) - 1\right]^2.$$

We take $\alpha = \beta = 2$, $T^* = 1$, and $\hbar_t = 0.01$.
The numerical results are compared with the Haar wavelet method, [10]. Tables 1–4, compare the error norms L_∞ and L_2 for the Sine–Cosine wavelet (SCW) and Haar wavelet (HW) methods at the different values x and t. Comparison between the exact and computed solutions $\Phi(x,t)$ and $\Psi(x,t)$ in the 3-dimensional graphs are shown in Figures 2 and 3, respectively. In Figures 4–7, we show the L_2 and L_∞ Errors for $\Phi(x,t)$ and $\Psi(x,t)$ at different space and time levels.

TABLE 1. The comparison among the exact and numerical solutions for $\Phi(0.475, t)$.

t	Φ_{exact}	SCW ($\ell^* = \kappa = 2$)		HW ($J = 3$)	
		Φ_{approx}	$\lvert\Phi_{exact} - \Phi_{approx}\rvert$	Φ_{approx}	$\lvert\Phi_{exact} - \Phi_{approx}\rvert$
0.1	0.223854	0.229491	$5.636470e-03$	0.216396	$7.457661e-03$
0.2	0.264987	0.269839	$4.851715e-03$	0.249831	$1.515627e-02$
0.3	0.309360	0.313166	$3.806702e-03$	0.284187	$2.517307e-02$
0.4	0.356250	0.358820	$2.570298e-03$	0.325065	$3.118473e-02$
0.5	0.404804	0.406035	$1.230867e-03$	0.364164	$4.064088e-02$
0.6	0.454106	0.453990	$1.162383e-04$	0.406758	$4.734797e-02$
0.7	0.503235	0.504209	$9.744409e-04$	0.448075	$5.515954e-02$
0.8	0.551331	0.551109	$2.220420e-04$	0.490346	$6.098543e-02$
0.9	0.597646	0.595123	$2.522691e-03$	0.530310	$6.733545e-02$
1	0.641568	0.637486	$4.081906e-03$	0.625770	$1.579795e-02$
L_∞ Error		$5.981972e-03$		$4.162985e-02$	
L_2 Error		$3.331779e-03$		$6.733545e-02$	

TABLE 2. The comparison among the exact and numerical solutions for $\Psi(0.475, t)$.

t	Ψ_{exact}	SCW ($\ell^* = \kappa = 2$)		HW ($J = 3$)	
		Ψ_{approx}	$\lvert\Psi_{exact} - \Psi_{approx}\rvert$	Ψ_{approx}	$\lvert\Psi_{exact} - \Psi_{approx}\rvert$
0.1	0.111927	0.114756	$2.829054e-03$	0.108233	$3.693724e-03$
0.2	0.132493	0.134927	$2.433295e-03$	0.124974	$7.519563e-03$
0.3	0.154680	0.156586	$1.906004e-03$	0.143706	$1.097422e-02$
0.4	0.178125	0.179407	$1.281757e-03$	0.164826	$1.329914e-02$
0.5	0.202402	0.203007	$6.050098e-04$	0.185488	$1.691435e-02$
0.6	0.227053	0.226977	$7.616807e-05$	0.207776	$1.927652e-02$
0.7	0.251617	0.251014	$6.030613e-04$	0.229886	$2.173131e-02$
0.8	0.275666	0.274465	$1.200731e-03$	0.252168	$2.349782e-02$
0.9	0.298823	0.297099	$1.723649e-03$	0.273673	$2.514959e-02$
1	0.320784	0.318696	$2.087995e-03$	0.314018	$6.765360e-03$
L_∞ Error		$3.000326e-03$		$2.514959e-02$	
L_2 Error		$1.752998e-03$		$1.651617e-02$	

TABLE 3. The comparison among the exact and numerical solutions for $\Phi(x, 1)$.

t	Φ_{exact}	SCW ($\ell^* = \kappa = 2$)		HW ($J = 3$)	
		Φ_{approx}	$\lvert\Phi_{exact} - \Phi_{approx}\rvert$	Φ_{approx}	$\lvert\Phi_{exact} - \Phi_{approx}\rvert$
0.125	0.690973	0.689037	$1.936460e-03$	0.703977	$1.300360e-02$
0.225	0.677319	0.674283	$3.035193e-03$	0.670138	$7.180178e-03$
0.325	0.663289	0.659474	$3.815090e-03$	0.647996	$1.529366e-02$
0.425	0.648896	0.644786	$4.110780e-03$	0.632435	$1.646176e-02$
0.525	0.634153	0.630021	$4.132548e-03$	0.619421	$1.473204e-02$
0.625	0.619075	0.615455	$3.619904e-03$	0.607530	$1.154478e-02$
0.725	0.603680	0.600596	$3.084689e-03$	0.597236	$6.444137e-03$
0.825	0.587989	0.586039	$1.949879e-03$	0.591094	$3.105750e-03$
0.925	0.572022	0.570607	$1.415732e-03$	0.593248	$2.122538e-02$
L_∞ Error		$4.203572e-03$		$2.664550e-02$	
L_2 Error		$3.036066e-03$		$1.457509e-02$	

TABLE 4. The comparison among the exact and numerical solutions for $\Psi(x,1)$.

t	Ψ_{exact}	SCW ($\ell^* = \kappa = 2$)		HW ($J = 3$)	
		Ψ_{approx}	$\lvert\Psi_{exact} - \Psi_{approx}\rvert$	Ψ_{approx}	$\lvert\Psi_{exact} - \Psi_{approx}\rvert$
0.125	0.345487	0.344524	$9.628590e-04$	0.350042	$4.555041e-03$
0.225	0.338659	0.337143	$1.515995e-03$	0.335095	$3.564335e-03$
0.325	0.331645	0.329760	$1.884463e-03$	0.324787	$6.857755e-03$
0.425	0.324448	0.322383	$2.065293e-03$	0.317280	$7.168556e-03$
0.525	0.317077	0.315001	$2.075183e-03$	0.310896	$6.180504e-03$
0.625	0.309538	0.307630	$1.907914e-03$	0.304979	$4.558660e-03$
0.725	0.301840	0.300244	$1.595654e-03$	0.299581	$2.259580e-03$
0.825	0.293994	0.292873	$1.120910e-03$	0.295379	$1.384505e-03$
0.925	0.286011	0.285460	$5.507815e-04$	0.293618	$7.606433e-03$
L_∞ Error		$2.087995e-03$		$9.719003e-03$	
L_2 Error		$1.522960e-03$		$5.724693e-03$	

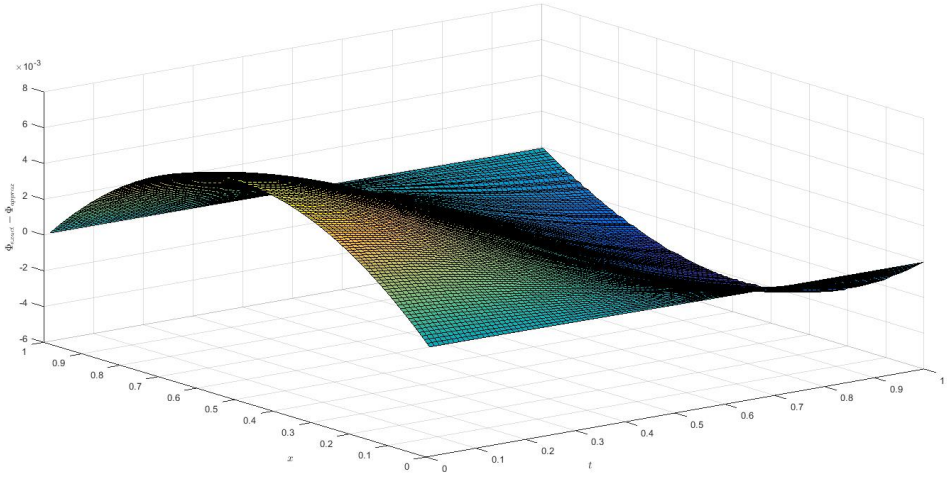

FIGURE 2. Comparison between the exact and computed solutions $\Phi(x,t)$ in the 3-dimensional graph, using the Sine–Cosine wavelets method, when $\ell^* = \kappa = 2$.

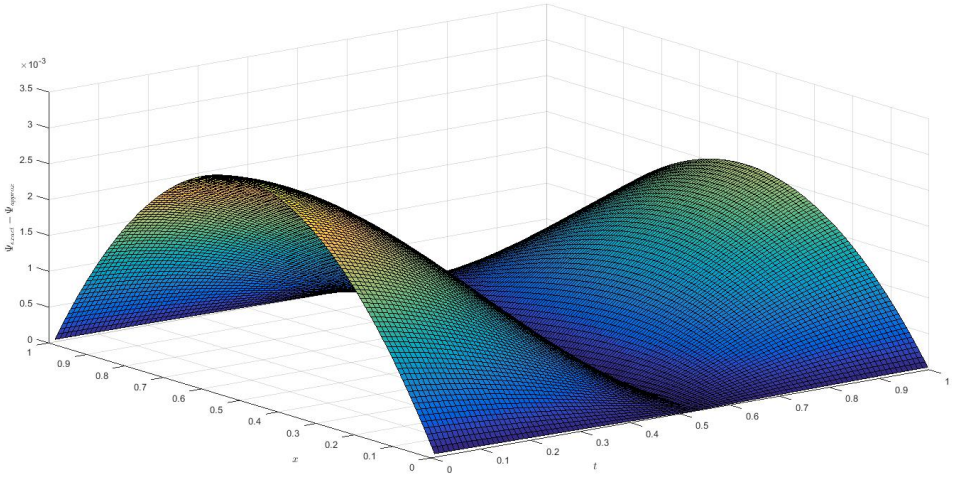

FIGURE 3. Comparison between the exact and computed solutions $\Psi(x,t)$ in the 3-dimensional graph, using the Sine–Cosine wavelets method, when $\ell^* = \kappa = 2$.

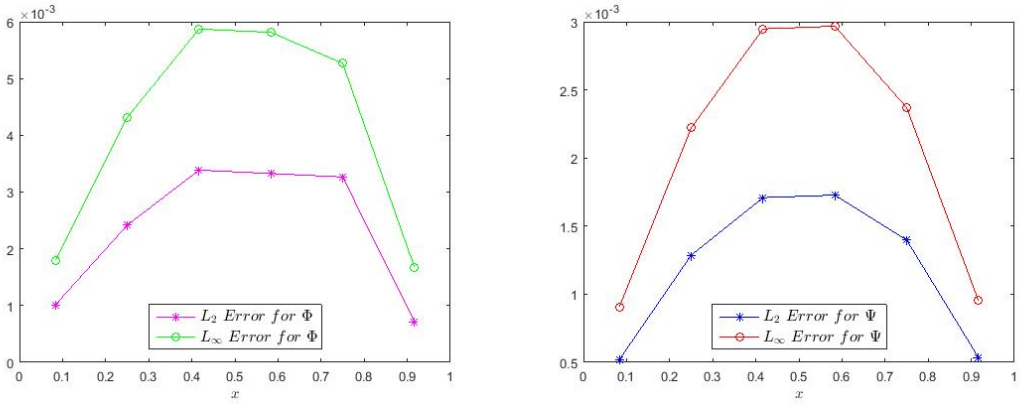

FIGURE 4. L_2 and L_∞ Errors for $\Phi(x,t)$ and $\Psi(x,t)$ with different space levels, using the Sine–Cosine wavelets method, when $\ell^* = \kappa = 1$.

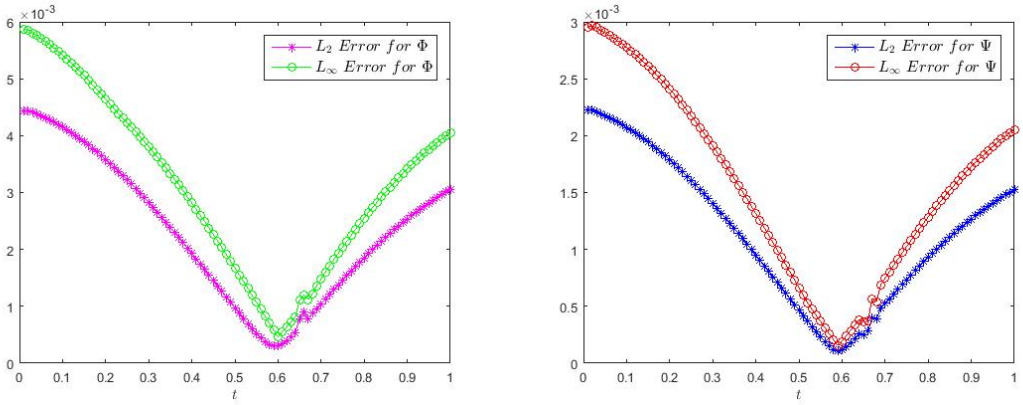

FIGURE 5. L_2 and L_∞ Errors for $\Phi(x,t)$ and $\Psi(x,t)$ at different time levels, using the Sine–Cosine wavelets method, when $\ell^* = \kappa = 1$.

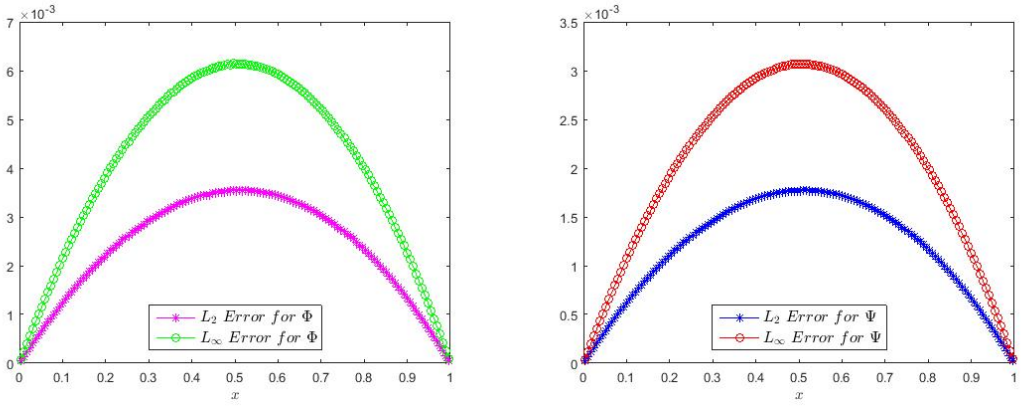

FIGURE 6. L_2 and L_∞ Errors for $\Phi(x,t)$ and $\Psi(x,t)$ with different space levels, using the Sine–Cosine wavelets method, when $\ell^* = \kappa = 2$.

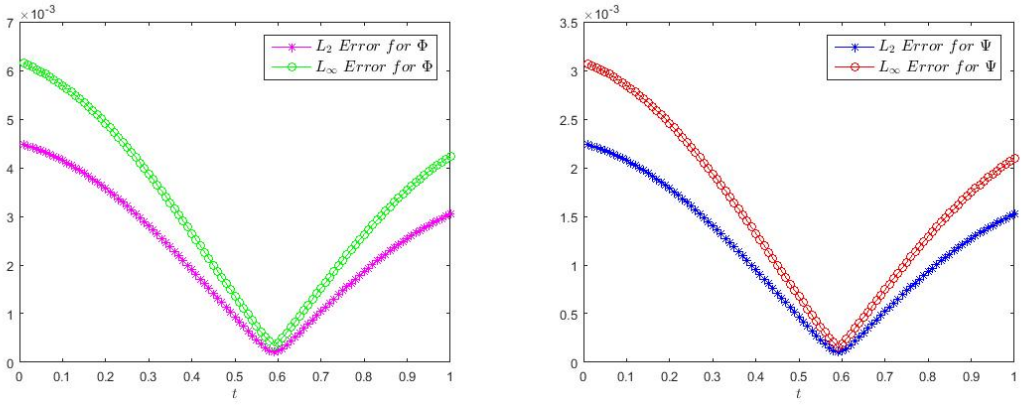

FIGURE 7. L_2 and L_∞ Errors for $\Phi(x,t)$ and $\Psi(x,t)$ at different time levels, using the Sine–Cosine wavelets method, when $\ell^* = \kappa = 2$.

CPU time consumption in Matlab for the SCW method is 123.097848 and for the HW method is 542.811835 seconds. These computational results show that our proposed method (SCW) is effective and

accurate in comparison with HW. Also, the SCW method is superior to the HW method due to the smaller CPU time.

5. Conclusion

In conclusion, in this paper, a numerical method for solving the nonlinear Belousov-Zhabotinsky reaction system was presented. As shown in the paper, the method is based upon hybrid function approximations; the time derivative was discretized by the finite difference method, and the spatial discretization was made by Sine–Cosine wavelets. The shown numerical results confirmed the accuracy of the method, and the plotted graphs confirmed the reliability of the applied methods. We also, compared this method with the Haar wavelet method to show the effectiveness of the Sine–Cosine wavelets method. The results of this comparison also confirm the accuracy of the method. Compared to the execution time of the program, the Sine–Cosine wavelets method has a better speed with low storage space. On the other hand, the operational matrix based on Sine–Cosine wavelets has a large number of zero components, which ensures good system performance and provides acceptable accuracy even with fewer collocation points. The methodology reported in this paper can be extended to solve other real-life problems. Due to the importance of the type of reaction diffusion equation in chemistry and the several physical phenomena, in future research, to improve the approximation to exact solution, new basis functions, and new numerical methods can be used; especially the focus will be on fractional order diffusion models.

References

[1] Shanks, N., (2001), Modeling biological systems: the Belousov–Zhabotinsky reaction, Foundations of Chemistry, 3 (1), pp. 33–53.
[2] Algehyne, E. A., Abd El-Rahman, M., Faridi, W. A., Asjad, M. I. and Eldin, S. M., (2023), Lie point symmetry infinitesimals, optimal system, power series solution, and modulational gain spectrum to the mathematical noyes–field model of nonlinear homogeneous oscillatory Belousov–Zhabotinsky reaction, Results in Physics, 44, p. 106123.
[3] Winfree, A. T., (1984), The prehistory of the Belousov-Zhabotinsky oscillator, Journal of Chemical Education, 61 (8), p. 661.
[4] Wang, M.-X., Xiong, S.-L. and Ye, Q.-X., (1994), Explicit wave front solutions of noyes-field systems for the Belousov-Zhabotinskii reaction, Journal of mathematical analysis and applications, 182 (3), pp. 705–717.
[5] Akinyemi, L., (2020), A fractional analysis of noyes–field model for the nonlinear Belousov–Zhabotinsky reaction, Computational and Applied Mathematics, 39 (3), p. 175.
[6] Karaagac, B., Esen, A., Ucar, Y. and Yagmurlu, N. M., (2023), A new outlook for analysis of noyes-field model for the nonlinear Belousov-Zhabotinsky reaction using operator splitting method, Computers & Mathematics with Applications, 136, pp. 127–135.
[7] Daubechies, I., (1992), Ten lectures on wavelets, SIAM.
[8] Chui, C. K., (2016), An introduction to wavelets, Elsevier.
[9] Azizi, N. and Pourgholi, R., (2021), Applications of Sine–Cosine wavelets method for solving Drinfel'd–Sokolov–Wilson system, Advances in Systems Science and Applications, 21 (3), pp. 75–90.
[10] Foadian, S., Pourgholi, R., Tabasi, S. H. and Damirchi, J., (2019), The inverse solution of the coupled nonlinear reaction–diffusion equations by the Haar wavelets, International Journal of Computer Mathematics, 96 (1), pp. 105–125.
[11] Idrees, S. and Saeed, U., (2022), Generalized Sine–Cosine wavelet method for Caputo–Hadamard fractional differential equations, Mathematical Methods in the Applied Sciences, 45 (16), pp. 9602–9621.
[12] Irfan, N. and Siddiqi, A., (2016), Sine–Cosine wavelets approach in numerical evaluation of Hankel transform for seismology, Applied Mathematical Modelling, vol. 40 (7-8), pp. 4900–4907.
[13] Heil, C., (1993), Ten lectures on wavelets (ingrid daubechies), SIAM Review, 35 (4), pp. 666–669.
[14] Bellman, R. E. and Kalaba, R. E., (1965). Quasilinearization and nonlinear boundary-value problems.

Saedeh Foadian received her B.Sc. degree in applied mathematics (2009), her M.Sc. degree in harmonic analysis (2012), and her Ph.D. degree in 2018 in Applied Mathematics at Damghan University, Iran. Her area of research is the numerical solution of linear and nonlinear partial differential equations.

Reza Pourgholi received his M.Sc. degree in 2001 and a Ph.D. degree in 2007 in Applied Mathematics from IUST, Tehran, Iran. He is now a full professor at Damghan University. His area of research is the numerical solution of inverse problems in partial differential equations.